Melting of a finite-sized two-dimensional colloidal crystal

Sayuri Tanaka, Yuma Oki, and Yasuyuki Kimura*
Department of Physics, School of Sciences, Kyushu University, 6-10-1 Hakozaki, Higashi-ku, Fukuoka 812-8581, Japan
(Received 16 January 2014; published 9 May 2014)

We have studied the melting process of a finite-sized two-dimensional colloidal crystal by video microscopy. The local area fraction ϕ and the local hexatic orientational order parameter ψ_6 have been evaluated for respective Voronoi cells in the crystal. The histogram of ϕ exhibits a peak and the peak ϕ continuously decreases with the time elapsed. The histogram of $|\psi_6|$ shows an abrupt broadening for $\phi < 0.65$. This critical value of ϕ is the transition point between the hexatic and dense liquid phases in finite crystal. We have also evaluated ϕ and $|\psi_6|$ as a function of the distance from the center of the crystal r. $\phi(r)$ is almost constant within the crystal and monotonously decreases with the time elapsed. $|\psi_6(r)|$ gradually decreases with r but there is the core with $|\psi_6| = 1$ at earlier time stage. The temporal change of the average ϕ within the crystal is qualitatively explained by the slow diffusion of the particles situated at the crystal edge. The steric repulsion between the particles within the crystal enhances the expansion rate of the crystal edge. Overall melting behavior is same in the crystals with different sizes. We have also studied the melting of a finite-sized crystal composed of soft-core particles by Brownian dynamics simulation and verified the finite-size effect on the melting process. The simulated behavior is qualitatively in good agreement with the experimental results.

DOI: 10.1103/PhysRevE.89.052305 PACS number(s): 82.70.Dd, 64.70.pv, 64.70.dj

I. INTRODUCTION

Colloidal crystals have been intensively studied as a model system of atomic and molecular crystals [1–3]. The advantage of utilizing colloidal particles as model is that one can study their structures and dynamics at the level of individual particles. Since the size of the particles is much larger than the atomic scale, the characteristic time scale of their dynamics becomes much slower and one can easily follow their dynamics under the microscope. The crystallization and melting processes of colloidal crystals have been studied in three dimensions with single-particle resolution [4–6]. These studies also offer important fundamental information for designing and building photonic crystals from the viewpoint of application [7].

The melting process of colloidal crystal drastically changes in lower dimensions where thermal fluctuation easily destroys the long-range positional order. The melting of two-dimensional crystal has intensively been studied theoretically and experimentally [8]. The most successful theoretical approach to this problem is the Kosterlitz-Thouless-Halperin-Nelson-Young (KTHNY) theory [9–12]. This theory predicts a two-step phase transition between crystal and liquid, including a hexatic phase as an intermediate phase. Even in the crystal phase, the translational order is quasi long range due to thermal fluctuation. The density correlation function decays as a power of interparticle distance. The hexatic phase exhibits short-ranged translational order and quasi-long-ranged hexatic orientational order. In the liquid phase, both orders become short ranged. The melting from the crystal to the hexatic phase is driven by the unbinding of dislocations and that from hexatic to liquid by unbinding of the disclination pairs [12].

The KTHNY scenario has theoretically been discussed by computer simulation [13–19]. Experimentally, the melting has been studied in charged colloids [20–22], size-tunable colloids [23,24], the colloids at the oil-water interface [25], plasma crystals [26,27], paramagnetic colloids under a magnetic field [28,29], and colloids under a laser light field [30]. In those studies, the melting has been realized by varying the concentration of particles [20–25] or the interaction between particles [26–30] in the equilibrium infinitely large systems in the scale of particle size.

However, the studies on the melting dynamics in a finite-sized colloidal crystal under the nonequilibrium condition are not so numerous [31–35] compared with that for nearly infinite crystals in equilibrium. Among them, the melting of a finite-sized crystal under short-range attraction which is induced by a depletion interaction has been reported [31]. Depending on the size of a crystal, the two kinds of melting processes have been observed. When the size of a crystal is larger than a certain threshold size, the crystal slowly melts from its edge. Otherwise, the crystal breaks into clusters and rapidly melts. However, the temporal growth of spatial inhomogeneity during the melting process of a finite-sized crystal has not been discussed much.

In this paper, we have studied the melting process of a finite-sized two-dimensional crystal composed of hard-sphere colloids. Since the concentration of the colloids around the crystal is very low, the observed process might be better called "sublimation." By introducing the local area fraction and the local hexatic orientational order parameter, we discussed the influence of crystal boundary and spatial inhomogeneity during the dynamic melting process. The dependence of the melting process on the initial crystal size has been also studied. The obtained experimental results are compared with those calculated by our Brownian dynamics simulation and the proceeding study under short-range attraction [31].

II. EXPERIMENT

In this study, we used uniform spherical silica particles 3.0 μm in diameter (Hipresica, UNK). They were stored in ultrapurified water with mix-bed ion-exchange resins before

*kimura@phys.kyushu-u.ac.jp

 ©2014 American Physical Society

use to avoid aggregation. The silica particles used in this study have silanol groups on their surfaces and they are slightly charged in pure water. Since the screening length is much smaller than the size of the particle, the interaction between them can be regarded as short-ranged repulsion or nearly hard-sphere-like repulsion. This is also supported by the fact that the aggregation of the particles has not been observed. The dilute silica solution was sandwiched between a slide glass and a cover glass. The one surface of the slide glass was deposited by indium tin oxide to enhance the laser heating over wide area. The slide glass was stored in the aqueous solution of sodium dodecyl sulfate at critical micelle concentration over night to prevent the adsorption of silica particles on the surface. The cover glass was burned at 500 °C to make its surface hydrophilic. The thickness of the sample cell was controlled by the quantity of the solution to fill the gap. The average resultant thickness of the cell was about 4 μm. The sides of the cell were enclosed by hydrophobic liquid blocker (Funakoshi) to avoid overflow, evaporation, and convection of the solution.

We artificially formed a single colloidal crystal of spherical silica particles with arbitrary size by thermal convection and thermal diffusion [36–38] in this study. Silica particles move toward the warmer region in water. Since this effect is usually tiny, we made the large temperature gradient by a strongly converged high power Nd:YVO_4 laser beam (wavelength 1064 nm, Spectra Physics) with an oil-immersion objective lens (Plan Apo VC, 60×, NA = 1.4, Nikon). This enables us to form a two-dimensional colloidal crystal with arbitrary size as shown in Figs. 1(a) and 1(c). However, we have not succeeded in increasing the area fraction of the particles up to the closest packing in two dimensions. When we increased the area fraction of the particles up to 0.85, some center particles were pushed out from the crystal by the pressure of the outer particles and attached the cell surface permanently. Therefore we started our experiments only from a certain area fraction smaller than 0.85.

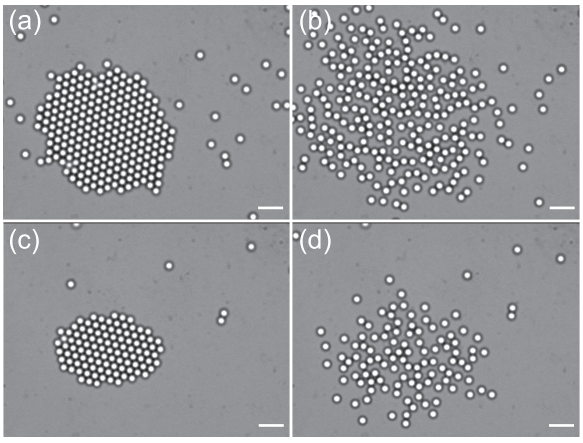

FIG. 1. Snapshots of the melting process of a large (L) and a small (S) colloidal crystal. [(a) and (c)] $t = 0$ s. [(b) and (d)] $t = 399$ s. The scale bars are 10 μm. The total number of particles within the crystal at $t = 0$ is 259 for the L crystal and 112 for the S crystal. The images are taken under a slightly defocused condition to avoid overlapping the individual particles' images. This makes it easy to evaluate the center position of the respective particles.

By turning off the laser beam, we abruptly switch off the attractive interaction which collects the particles. Then the crystal starts to melt by diffusion of the particles from the crystal edge. This situation corresponds to superheating of the crystal far above the melting temperature. The melting process was observed under an inverted optical microscope (TE2000-U, Nikon) with the same objective lens used for laser heating. The images were captured by a monochrome charge-coupled-device camera (ADP-240, Flovel, 12-bit) at 10 frames/s. After correcting the brightness of images and subtracting the background, the images were binarized and the center position of the particles were tracked with Image J.

For further analysis of the melting process, we divided the space into a number of regions called Voronoi cells. For the center position of each particle, a Voronoi cell is a corresponding region consisting of all points closer to this center point than to any other. From the Voronoi map, we calculated the local area fraction ϕ as the area ratio of a particle, $1.5^2\pi\,\mu\mathrm{m}^2$, to a Voronoi cell for respective cells as shown in Fig. 2. The local ϕ is proportional to the local number density of the particles.

We also evaluated the local hexatic orientation order parameter ψ_6 for the respective Voronoi cell including the j-th particles at $\boldsymbol{r}_j$ as

$$\psi_6(\boldsymbol{r}_j,t) = \frac{1}{N}\sum_{k=1}^{N}\exp(6i\theta(\boldsymbol{r}_{jk},t)), \tag{1}$$

where $\theta(\boldsymbol{r}_{jk},t)$ is the angle between the vector connecting j-th and k-th nearest-neighboring particle $\boldsymbol{r}_{jk}$ and the horizontal axis of the captured images and N is the number of the neighboring particles to the j-th particle. If the cell has the perfect sixfold rotational symmetry, $\psi_6 = 1$. The examples of the spatial distribution of $|\psi_6|$ are shown in Fig. 3.

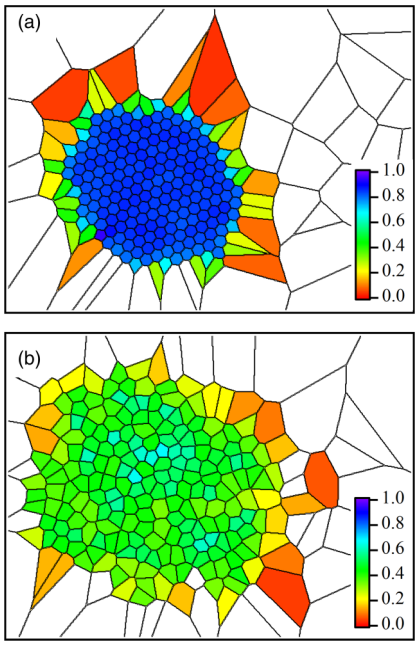

FIG. 2. (Color online) Distribution of the local area fraction ϕ in an L crystal. (a) $t = 0$ s. (b) $t = 399$ s. The polygons are the Voronoi cells of the respective particles.

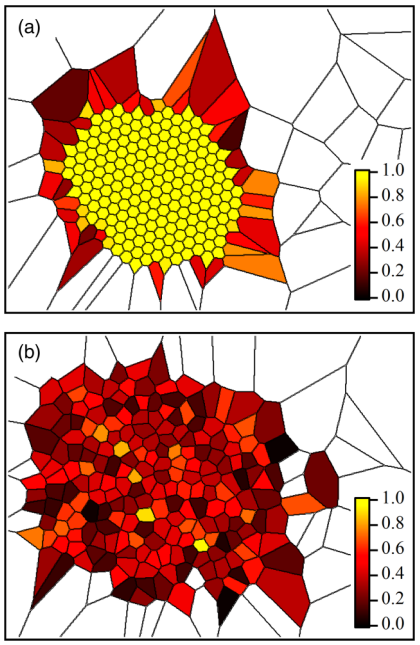

FIG. 3. (Color online) Distribution of the hexatic orientational order parameter $|\psi_6|$ in an L crystal. (a) $t = 0$ s. (b) $t = 399$ s. The polygons are the Voronoi cells of the respective particles.

III. TEMPORAL CHANGE IN HISTOGRAM OF LOCAL PARAMETERS ϕ AND ψ_6

We study the histogram of the local area fraction ϕ over the crystal. Figures 4(a) and 4(b) respectively show the temporal change in the histogram of ϕ for a large (L) and a small (S) crystal. These graphs respectively exhibit peaks at respective time points. The value of ϕ at the peak decreases from 0.82 to 0.5 with time t. The peak height also continuously decreases and the distribution becomes broader as the time elapsed. We cannot identify any transition behavior from the temporal change in the histogram of ϕ.

We also study the temporal change in the histogram of local hexatic orientational order parameter $|\psi_6|$ as shown in Figs. 4(c) and 4(d) for respective crystals. These graphs exhibit clear peaks at $|\psi_6| > 0.8$ at the earlier time stage. However, the peak broadens and the data largely scatter around 0.4 at the later time stage. A similar change in the histogram of $|\psi_6|$ has been reported for the shear-induced melting of a three-dimensional colloidal crystal [6]. Also, in the infinitely large system, the coexistence of two characteristic distributions in $|\psi_6|$ has been reported during the melting process [21,39].

The peak in the histogram of $|\psi_6|$ disappears at around $t = 80$ s for the L crystal and $t = 50$ s for the S crystal. The dynamic melting of hexatic phase might occur around this time point and the hexatic and liquid phase coexist at this point. This is the reason that the peak disappears at this moment and a broad peak reappears again as the time elapsed. Although the coexistence of two phases seems to indicate that the hexatic and liquid phase transition is first order, this transition is considered to be continuous in the KTHNY scenario. On the other hand, Bernard and Krauth recently have found that the hexatic-to-liquid phase transition in the two-dimensional hard-disk system is first order by use of the Monte Carlo simulation for a larger system [40]. The experimentally observed coexistence is mainly due to the nonequilibrium inhomogeneity in our system but may be partly due to the first-order hexatic-liquid phase transition.

We find that the corresponding peak ϕ at this time point is about 0.65 irrespective of the crystal size, as indicated by lines in Figs. 4(a) and 4(b). This indicates that the average

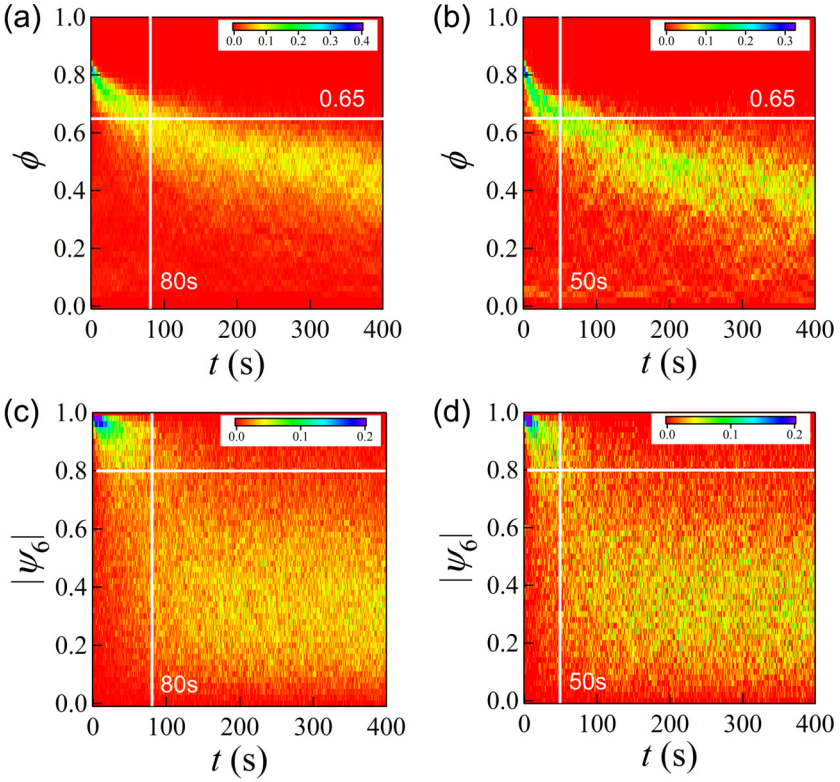

FIG. 4. (Color online) Temporal change in the histogram of ϕ and $|\psi_6|$ for an L crystal and an S crystal. (a) ϕ in the L crystal. (b) ϕ in the S crystal. (c) $|\psi_6|$ in the L crystal. (d) $|\psi_6|$ in the S crystal. The transition between the hexatic and liquid phases occurs about 80 s for the L crystal and dabout 50 s for the S crystal as indicated by the lines in (c) and (d). The corresponding ϕ is about 0.65 irrespective of the crystal size as shown in the lines in (a) and (b).

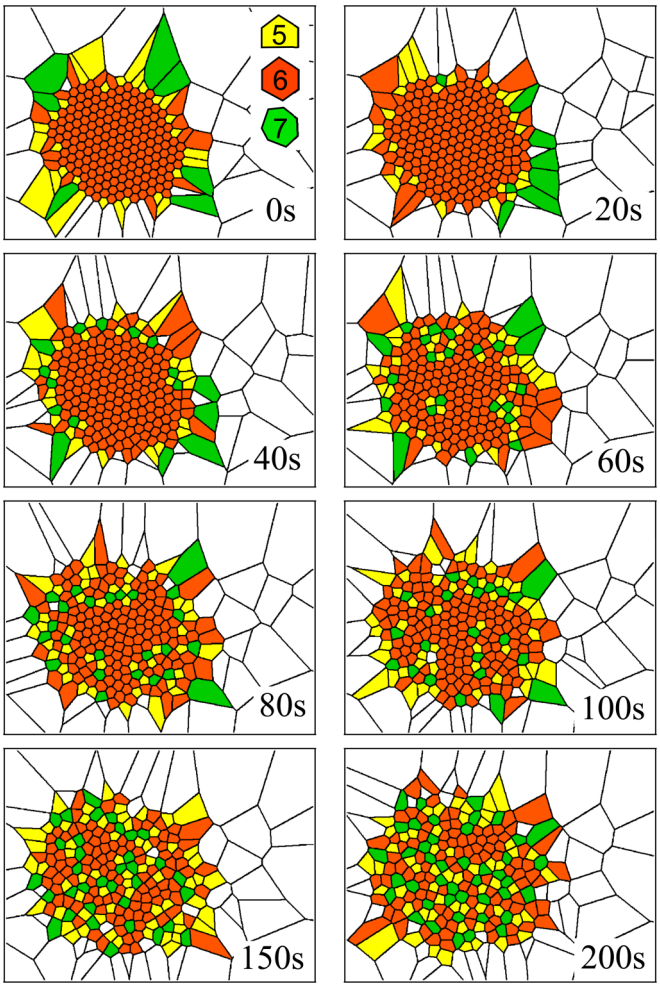

FIG. 5. (Color online) Temporal change in the spatial distribution of the number of the nearest neighbors. The cells which have fifth-, sixth-, and seventh-nearest neighbors are represented in different colors.

melting behavior does not depend on the size of crystal. The only difference between the L and S crystals is that in time scale. The time necessary to expand to the same ϕ depends on the initial crystal size. Since the overall behavior of the melting process does not strongly depend on the crystal size, we only present the experimental result on the L crystal in the following discussion.

In order to observe the dynamic melting process of the hexatic phase, we studied the two-dimensional spatial distribution of the number of the nearest neighboring (NN) particles as shown in Fig. 5. According to the experimental result in infinitely large crystals, melting of the hexatic phase proceeds by the dissociation of the pair of 5- and 7-NN disclinations [21]. In our experiment, melting proceeds with the repeated creation of defects at the edge of the crystal and their diffusion to the center region. The growth of chains of 5- and 7-NN pairs from the edge of the crystal has been also observed (60, 80, and 100 s in Fig. 5).

The dependence of the fraction of 5-, 6- and 7-NN pairs on time t is shown in Fig. 6. The fraction of the 6-NN pair decreases with time and approaches 0.5. The number of 5- and 7-NN pairs increases with time and respectively approaches

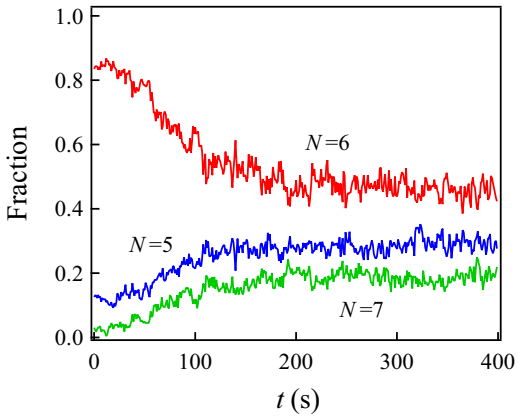

FIG. 6. (Color online) Dependence of the fraction of the number of the nearest-neighboring particles on time t.

0.3 and 0.2. Since the transition from the hexatic to the liquid phase undergoes the dissociation of 5-NN and 7-NN pairs [21], the fraction of 5- and 7-NN pairs is expected to be the same. However, there is an imbalance in the number of the pairs in Fig. 6. Such an asymmetry has been also observed in the infinite system [23]. However, in this study, this is mainly due to the fact that the boundary particles have a smaller NN pair as clearly seen at 0 s and 20 s in Fig. 5, and the number of particles at boundary is relatively large in our finite system.

IV. RADIAL DISTRIBUTION OF LOCAL PARAMETERS $\phi(r)$ AND $\psi_6(r)$

The radial distribution of local parameters $\phi(r)$ and $\psi_6(r)$ have been studied to examine the spatial inhomogeneity within the crystal (hereafter we call it cluster). Those two values are respectively evaluated by $\phi(r) = \sum_{r \leqslant r_i \leqslant r+\Delta r} \phi(r_i)/M$ and $|\psi_6(r)| = \sum_{r \leqslant r_i \leqslant r+\Delta r} |\psi_6(r_i)|/M$, where M is the number of the particles whose radial position r_i satisfy $r \leqslant r_i \leqslant r + \Delta r$. The calculated $\phi(r)$ and $|\psi_6(r)|$ are respectively shown in Figs. 7(a) and 7(b). $\phi(r)$ exhibits an almost constant value within the cluster, and this constant value of ϕ monotonously decreases with the time elapsed. In order to evaluate the size of the cluster and the average density within the cluster, we fitted the radial profile $\phi(r)$ by

$$\phi(r) = A \tanh\left(\frac{r_0 - r}{\xi}\right) + C, \tag{2}$$

where A is the amplitude, r_0 is the radius of the cluster, ξ is the half width of the edge, and C is constant. The best-fitted curves of Eq. (2) to data at respective time points are drawn as the solid curves in Fig. 7(a). Although this profile is usually used to analyze the equilibrium density profile across the boundary between two coexisting phases, the agreement is good except for the longer elapsed time.

The dependence of r_0, ξ, and ϕ_0 (ϕ at $r = 0$) on the elapsed time t are shown in Figs. 8(a) and 8(b). The value of r_0 can be regarded as the size of the cluster and increases with t. The value of ξ is the measure of the roughness of the boundary of the cluster. ξ is almost constant as large as one or two times of the particle's diameter. ϕ_0 is a decreasing function of t.

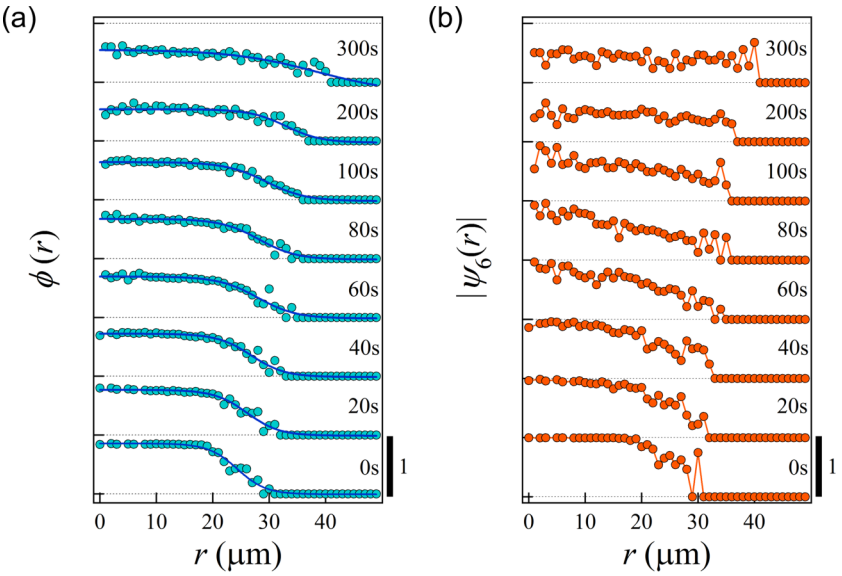

FIG. 7. (Color online) Temporal change in the radial distribution of (a) the local area fraction $\phi(r)$ and (b) the local hexatic orientational order parameter $|\psi_6(r)|$ in the L crystal. The solid lines in (a) are the best-fitted curves of Eq. (2).

We discuss this temporal change using a simple model: The boundary position follows the diffusion process and the density within the cluster is independent of r. With this simple assumption, r_0 is given by

$$r_0(t) \simeq \alpha + \beta\sqrt{t}, \tag{3}$$

where α and β are constant. The number of the particles within the crystal is conserved and the temporal change $\phi_0(t) = \phi(r = 0,t)$ is given by

$$\frac{\phi_0(t)}{\phi_0(0)} = \frac{\alpha^2}{r_0^2} \simeq (1 + \gamma\sqrt{t})^{-2}, \tag{4}$$

where γ is the constant.

Instead of Eq. (4), we fitted the time dependence of $\phi_0(t)/\phi_0(0)$ shown in Fig. 8(b) by

$$\frac{\phi_0(t)}{\phi_0(0)} = (1 + a_1 t^{a_2})^{-2}. \tag{5}$$

The best-fitted values are $a_1 = 1.09 \times 10^{-2}$ and $a_2 = 0.558$. The best-fitted curve is shown as the solid line in Fig. 8(b). With the best-fitted value $a_2 = 0.558$, we can also fit $r_0(t) = a_3 + a_4 t^{0.558}$ to data with $a_3 = 22.92$ and $a_4 = 0.517$ as shown in the solid line in Fig. 8(a). The obtained exponent $a_2 = 0.558$ is a little bit larger than 0.5. This is partly due to the repulsion between the interior particles. This repulsive effect will be discussed theoretically by use of a Brownian dynamics simulation in the next section. Although the relation $a_1 = a_4/a_3$ is expected to hold from Eqs. (3) and (4), the growth rate of r_0 is larger than that estimated from the decrease of the average density ϕ_0. This indicates that the expansion rate of the cluster differs from the free diffusion rate outside of the cluster. Although the dependence of $\phi_0(t)$ is mainly determined by the expansion rate of the cluster, the size r_0 is determined by the whole profile of $\phi(r)$, including the exterior particles near the boundary. This makes the size r_0 greater than that expected from the dense part of the cluster, and the growth rate of r_0 becomes larger on appearance. This is also the reason that the fitting of Eq. (2) to data becomes worse at later time stages.

The radial distribution $|\psi_6(r)|$ exhibits the flat part with $|\psi_6(r)| \simeq 1$ at the center region of the cluster, but $|\psi_6(r)|$ at the outer region decreases with r for $0 < t < 80$ s. For $t > 80$ s, $|\psi_6(r)|$ at the center of the cluster becomes smaller than 1. This corresponds the distribution of 5- and 7-NN particles in Fig. 5. These particles are distributed at the outer side of the cluster and invade into the inner region as time elapses. At longer time periods, $|\psi_6(r)|$ approaches 0.5 over the whole distance within the cluster. To visualize this change, the temporal change of the two characteristic values are shown in Fig. 9: The radius of the

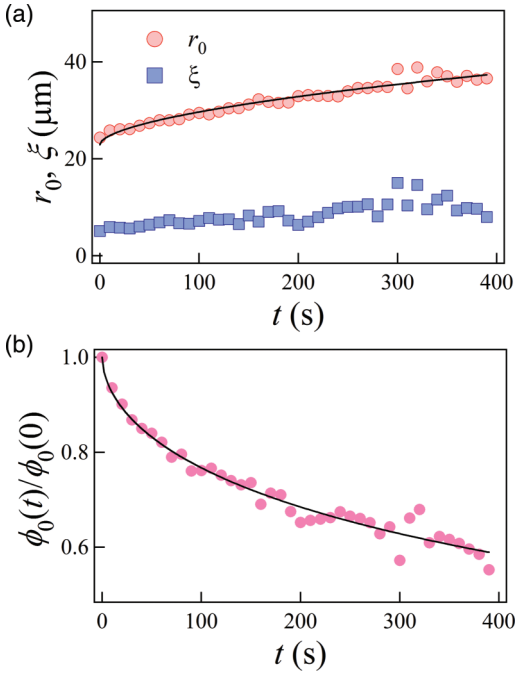

FIG. 8. (Color online) Temporal change of the radius of the cluster r_0, the boundary width ξ, and ϕ at the center of the cluster ϕ_0. The best-fitted lines, $r_0(t) = 22.92 + 0.517t^{0.558}$ and $\phi_0(t)/\phi_0(0) = (1 + 1.09 \times 10^{-2} t^{0.558})^{-2}$, are respectively drawn as the solid lines in (a) and (b).

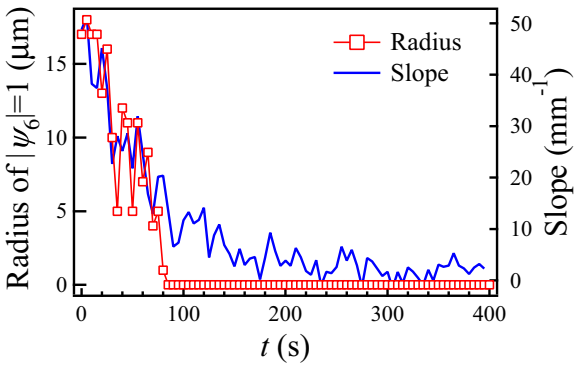

FIG. 9. (Color online) Temporal change of the radius of the area of $|\psi_6| = 1$ and the slope of $|\psi_6|$ in the cluster. The area of $|\psi_6| = 1$ disappears at around $t = 80$ s and the average slope monotonously decreases with t. The transition from the hexatic to the liquid phase is considered to occur at $t = 80$ s.

region with $|\psi_6| = 1$ and the average slope of the declined part within the cluster. The $|\psi_6| = 1$ area monotonously shrinks and disappears at about $t = 80$ s. This time point agrees with that when the histogram of $|\psi_6|$ drastically changes. The slope continuously decreases with time and approaches zero.

V. BROWNIAN DYNAMICS SIMULATION OF THE MELTING OF A FINITE-SIZED CRYSTAL

We also study the melting process of a finite-sized colloidal crystal by use of a Brownian dynamics simulation. In our simulation, the soft repulsive interaction between the particles, $U(r_{ij}) = 4\varepsilon(d/r_{ij})^{12}$, is only taken into account, where ε (>0) is the magnitude of the interaction, d is the diameter of the particle, and r_{ij} is the interparticle distance between the i-th and j-th particles. We have not taken into account the hydrodynamic and electrostatic ones. The dynamics of the respective particles follow the Langevin equations in the viscous limit as

$$\zeta \frac{d\boldsymbol{r}_i}{dt} = \sum_{i \neq j} 48\varepsilon \left(\frac{d}{r_{ij}}\right)^{12} \frac{\boldsymbol{e}_{ij}}{r_{ij}} + \boldsymbol{f}_i^B, \tag{6}$$

where $\boldsymbol{r}_i$ is the position of the i-th particle, ζ is the friction coefficient, $\boldsymbol{e}_{ij}$ is the unit vector parallel to $\boldsymbol{r}_{ij}$, and $\boldsymbol{f}_i^B$ is the random force acting on the i-th particle. $\boldsymbol{f}_i^B$ satisfies $\langle \boldsymbol{f}_i^B(t) \rangle = 0$ and $\langle \boldsymbol{f}_i^B(t') \boldsymbol{f}_i^B(t'') \rangle = 2\zeta k_B T \delta(t' - t'')$, where $\langle \cdots \rangle$ represents ensemble average, k_B is the Boltzmann constant, and T is the absolute temperature. We used the dimensionless form of Eq. (6) for simulation. The unit scales are d for length, $t_d = d^2/D$ for time (D is the diffusion constant of the particle, which is given by $D = k_B T/\zeta$), and $k_B T$ for energy. In our simulation, the time step is 10^{-5}, the number of particles is 169, and $\varepsilon = 2.0$. We set the initial arrangement of the particles to the hexagonal one and the initial interparticle separation to $1.05d$. This distance corresponds the experimental initial area fraction $\phi = 0.83$.

The results of simulation corresponding to the experimental ones, Figs. 4, 7, and 8, are respectively shown in Figs. 10–12. We can also note that the time point at the hexatic-liquid transition is about 7000 and the corresponding ϕ is about 0.63. This value is closed to our experimental value of 0.65 in finite-sized clusters and that in the bulk of about $\phi = 0.7$. The value is also close to the bulk value in a similar system [21]. The simulated radial distribution of $\phi(r)$ and $|\psi_6(r)|$ in Fig. 11 also makes a qualitative agreement with the experimental data in Fig. 7. In the middle time stage, the experimental result of $|\psi_6(r)|$ exhibits the gradual decrease with r while $\phi(r)$ maintains an almost uniform value within the cluster. This characteristic radial dependence of $|\psi_6|$ is also reproduced in the simulation.

The temporal variation of the fitting parameters is quantitatively in agreement with experimental data. The time dependence of ϕ_0 is well fitted by Eq. (5) with $a_1 = 8.23 \times 10^{-4}$ and $a_2 = 0.578$ as shown in the solid line in Fig. 12(b). The time dependence of the cluster size r_0 is also well fitted by $r_0 = 19.57 + 1.81 \times 10^{-2} t^{0.578}$ as shown in the solid line in Fig. 12(a). The ratio of the best-fitted values $1.81 \times 10^{-2}/19.57$ is close to a_1 but is a bit larger than a_1. The best-fitted value of $a_2 = 0.578$ is close to the experimental value of $a_2 = 0.558$. This indicates that the introduction of a repulsive interaction accelerates the melting process.

VI. DISCUSSION

As discussed in the previous section, the short-range repulsive interaction and finite-size effect are essential for the melting dynamics in our system. We briefly compare the result of pure diffusion of a finite-sized single cluster composed of sizeless particles without interaction. The temporal variation

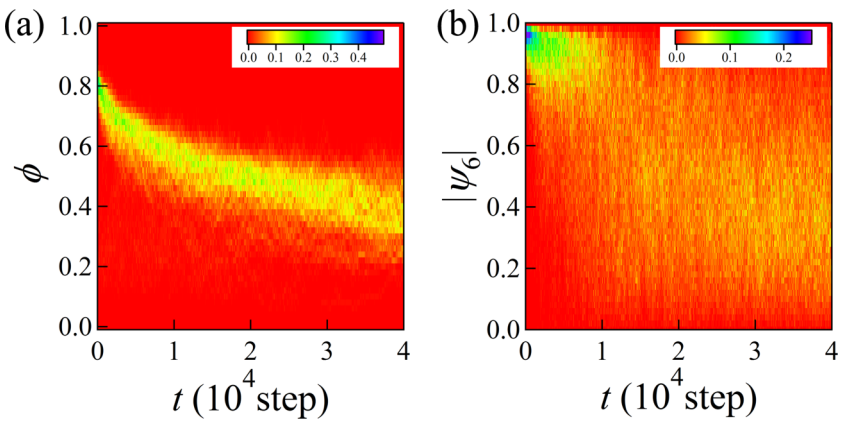

FIG. 10. (Color online) Temporal change in the histogram of ϕ and $|\psi_6|$ obtained by use of a Brownian dynamics simulation. (a) ϕ; (b) $|\psi_6|$.

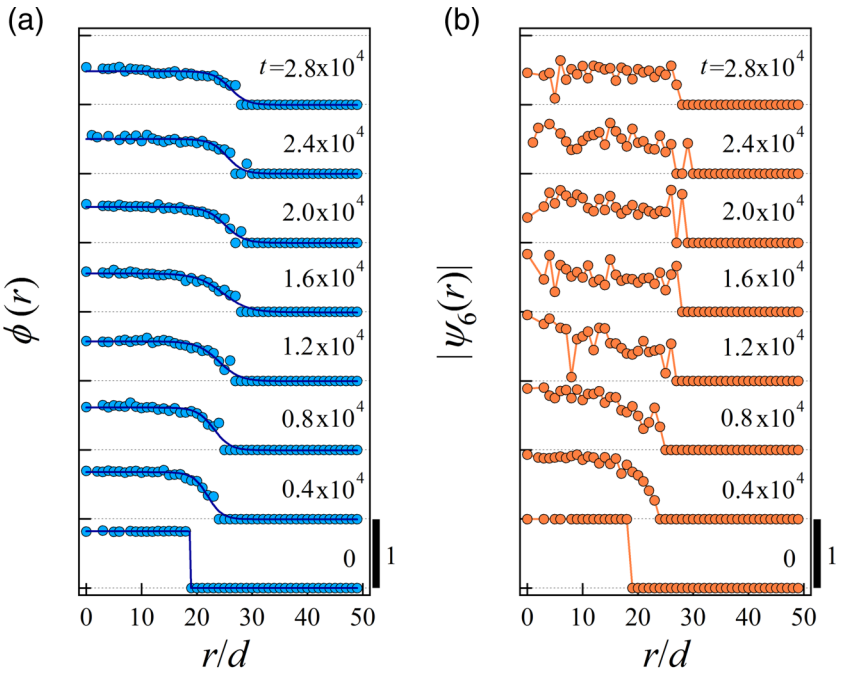

FIG. 11. (Color online) Temporal change in the radial distribution of $\phi(r)$ and $|\psi_6(r)|$ obtained by use of a Brownian dynamics simulation. (a) $\phi(r)$; (b) $|\psi_6(r)|$. The solid lines in (a) are the best-fitted curves of Eq. (2).

of density $\phi(r,t)$ governed by the diffusion equation (where D is the diffusion constant),

$$\frac{\partial\phi(r,t)}{dt} = D\frac{\partial^2\phi(r,t)}{dr^2}, \tag{7}$$

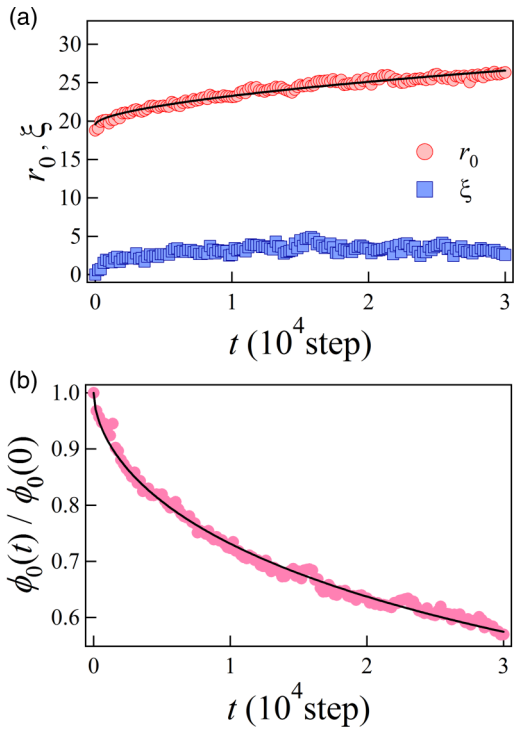

FIG. 12. (Color online) Temporal change in the size of a cluster r_0, the boundary width ξ, and ϕ at the center of the crystal ϕ_0. The best-fitted lines, $r_0(t) = 19.57 + 1.81 \times 10^{-2}t^{0.578}$ and $\phi_0(t)/\phi_0(0) = (1 + 8.23 \times 10^{-4}t^{0.578})^{-2}$, are respectively drawn as the solid lines in (a) and (b).

with the initial condition,

$$\phi(r,0) = \theta(r_0 - r) = \begin{cases} 1 & (r_0 \geqslant r) \\ 0 & (r_0 < r) \end{cases}, \tag{8}$$

is given by

$$\phi(r,t) = \frac{1}{2}\left[\mathrm{erf}\left(\frac{r_0 - r}{2\sqrt{Dt}}\right) + \mathrm{erf}\left(\frac{r_0 + r}{2\sqrt{Dt}}\right)\right], \tag{9}$$

where r_0 is the initial radius of the cluster and $\mathrm{erf}(x)$ is the Gaussian error function defined by

$$\mathrm{erf}(x) = \frac{2}{\sqrt{\pi}}\int_0^x \exp(-u^2)du. \tag{10}$$

The temporal variation of Eq. (9) is schematically shown in Fig. 13(b). At the earlier time stage, the edge position of the cluster is almost same and the region with $\phi = 1$ rapidly shrinks. Then, with the time t elapsed, the profile of $\phi(r)$ approaches Gaussian. This differs from that observed in our study as shown in Fig. 13(a).

On the other hand, when the attractive interaction exists as reported in Ref. [31], the size of the crystal decreases while keeping a high ϕ value which corresponds to the crystal phase and the width of the boundary is about two layers, as schematically shown in Fig. 13(c). After the size of the crystal becomes smaller than a certain critical value, it rapidly decomposes into small dense clusters.

In our system, the expansion of the cluster is governed by the diffusion of the outermost particles. Since the cooperative diffusion of the particles within the cluster is large, this enables us to equilibrate the density of the particles within the cluster much faster than the expansion speed. Therefore, the density at the interior of the cluster is almost constant and the system can be regarded as an infinite system with the same ϕ. The comparison between three systems suggests that the dynamics

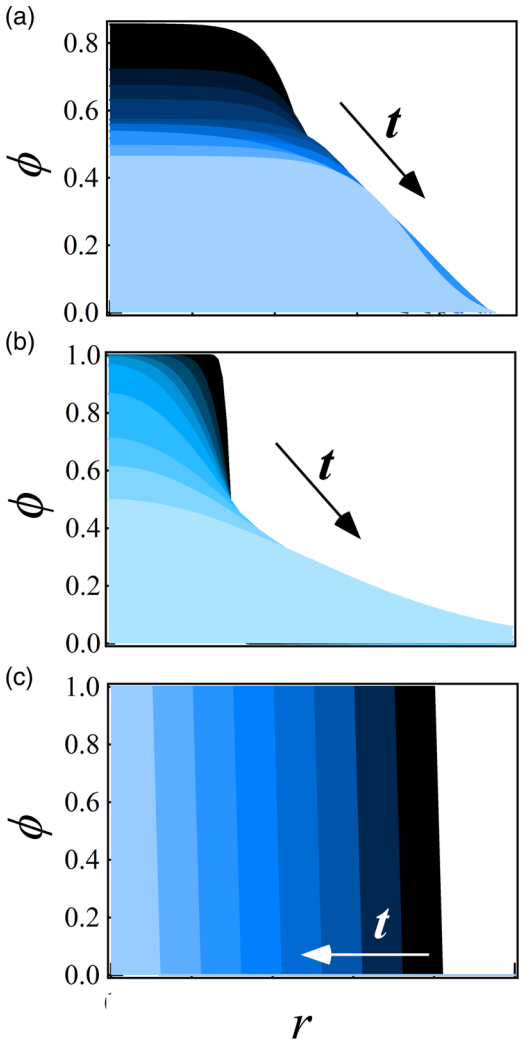

FIG. 13. (Color online) Schematic temporal change of the radial distribution of the area fraction $\phi(r)$. (a) Experimental result in the present study (short-range repulsion). (b) Simple diffusion (pointlike particle without interaction). (c) Previous experimental result (short-range attraction).

of the melting process is largely influenced by the interaction between particles, especially in the finite-sized system.

VII. CONCLUSIONS

We have studied the melting process of an isolated two-dimensional colloidal crystal (or cluster) with single particle resolution. The use of the thermophoretic force to collect colloidal particles enabled us to form an isolated nearly close-packed cluster without defects. We evaluated the local area fraction ϕ and local hexatic orientation order parameter ψ_6 for respective Voronoi cells. From the temporal variation of the histogram of ϕ and $|\psi_6|$, the distribution of $|\psi_6|$ abruptly changed at $\phi = 0.65$. The overall manner of change does not depend on the initial size of the crystal. From the radial distribution of ϕ and $|\psi_6|$, the melting process was found to differ markedly from that with attractive interaction or without interaction. The decrease of the area fraction was limited by the diffusion of the most-outer particles. The distribution of ϕ within the cluster was almost uniform and the average ϕ monotonously decreased with time. The experimentally obtained results were qualitatively reproduced by Brownian dynamics simulation of the particles interacting via soft-core repulsion. The precise melting process by controlling the interaction between particles in colloidal systems is valuable to elucidate the melting mechanism in atomic systems.

ACKNOWLEDGMENTS

The authors thank M. Ichikawa and Y. Iwashita for their valuable comments. This work was supported by a Grant-in-Aid for Scientific Research, KAKENHI Grants No. 23340123 and No. 25103011, from JSPS. Y.K. also thanks the support from Innovative Areas, “Fluctuation & Structure” (Grant No. 25610125), from MEXT, Japan.

[1] P. Pieranski, Contemp. Phys. **24**, 25 (1983).
[2] A. D. Dinsmore, J. C. Crocker, and A. G. Yodh, Curr. Opin. Colloid Interface Sci. **3**, 5 (1998).
[3] A. P. Gast and W. B. Russel, Phys. Today **51**, 24 (1998).
[4] W. K. Kegel and A. van Blaaderen, Science **287**, 290 (2000).
[5] U. Gasser, E. R. Weeks, A. Schofield, P. N. Pusey, and D. A. Weitz, Science **292**, 258 (2001).
[6] Y. L. Wu, D. Derks, A. V. Blaaderen, and A. Imhof, Proc. Natl. Acad. Sci. USA **106**, 10564 (2009).
[7] A. P. Hynninen, J. H. J. Thijssen, C. M. Vermolen, M. Dijkstra, and A. van Blaaderen, Nat. Mater. **6**, 202 (2007).
[8] K. J. Strandburg, Rev. Mod. Phys. **60**, 161 (1988).
[9] J. M. Kosterlitz and D. J. Thouless, J. Phys. C **6**, 1181 (1973).
[10] D. R. Nelson and B. I. Halperin, Phys. Rev. B **19**, 2457 (1979).
[11] A. P. Young, Phys. Rev. B **19**, 1855 (1979).
[12] D. R. Nelson, *Defects and Geometery in Condensed Matter Physics* (Cambridge University Press, Cambridge, 2002).
[13] K. Chen, T. Kaplan, and M. Mostoller, Phys. Rev. Lett. **74**, 4019 (1995).
[14] F. L. Somer, Jr., G. S. Canright, T. Kaplan, K. Chen, and M. Mostoller, Phys. Rev. Lett. **79**, 3431 (1997).
[15] A. Jaster, Phys. Rev. E **59**, 2594 (1999).
[16] C. H. Mak, Phys. Rev. E **73**, 065104 (2006).
[17] S. Z. Lin, B. Zheng, and S. Trimper, Phys. Rev. E **73**, 066106 (2006).
[18] W. K. Qi, Z. Wang, Y. Han, and Y. Chen, J. Chem. Phys. **133**, 234508 (2010).
[19] S. Prestipino, F. Saija, and P. V. Giaquinta, Phys. Rev. Lett. **106**, 235701 (2011).
[20] A. H. Marcus and S. A. Rice, Phys. Rev. Lett. **77**, 2577 (1996).

[21] A. H. Marcus and S. A. Rice, Phys. Rev. E **55**, 637 (1997).
[22] A. H. Marcus, J. Schofield, and S. A. Rice, Phys. Rev. E **60**, 5725 (1999).
[23] Y. Han, N. Y. Ha, A. M. Alsayed, and A. G. Yodh, Phys. Rev. E **77**, 041406 (2008).
[24] Z. Wang, A. M. Alsayed, A. G. Yodh, and Y. Han, J. Chem. Phys. **132**, 154501 (2010).
[25] B.-J. Lin and L.-J. Chen, J. Chem. Phys. **126**, 034706 (2007).
[26] R. A. Quinn and J. Goree, Phys. Rev. E **64**, 051404 (2001).
[27] R. Ichiki, Y. Ivanov, M. Wolter, Y. Kawai, and A. Melzer, Phys. Rev. E **70**, 066404 (2004).
[28] K. Zahn, R. Lenke, and G. Maret, Phys. Rev. Lett. **82**, 2721 (1999).
[29] K. Zahn and G. Maret, Phys. Rev. Lett. **85**, 3656 (2000).
[30] Q. H. Wei, C. Bechinger, D. Rudhardt, and P. Leiderer, Phys. Rev. Lett. **81**, 2606 (1998).
[31] J. R. Savage, D. W. Blair, R. A. Guyer, and A. D. Dinsmore, Science **314**, 795 (2006).
[32] J. R. Savage and A. D. Dinsmore, Phys. Rev. Lett. **102**, 198302 (2009).
[33] L. J. Moore, R. D. Dear, M. D. Summers, R. P. A. Dullens, and G. A. D. Ritchie, Nano Lett. **10**, 4266 (2010).
[34] Z. Wang, F. Wang, Y. Peng, Z. Zheng, and Y. Hang, Science **338**, 87 (2012).
[35] C. S. Dutcher, T. J. Woehl, N. H. Talken, and W. D. Ristenpart, Phys. Rev. Lett. **111**, 128302 (2013).
[36] S. Duhr and D. Braun, Appl. Phys. Lett. **86**, 131921 (2005).
[37] F. M. Weinert and D. Braun, Phys. Rev. Lett. **101**, 168301 (2008).
[38] R. Di Leonardo, F. Ianni, and G. Ruocco, Langmuir **25**, 4247 (2009).
[39] P. Karnchanaphanurach, B. Lin, and S. A. Rice, Phys. Rev. E **61**, 4036 (2000).
[40] E. P. Bernard and W. Krauth, Phys. Rev. Lett. **107**, 155704 (2011).